

A METHODOLOGY FOR WAVE-TO-WIRE WEC SIMULATIONS

Helen Bailey¹
University of Victoria
BC, Canada

Juan P Ortiz
University of Victoria
BC, Canada

Bryson Robertson
University of Victoria
BC, Canada

Bradley J Buckham
University of Victoria
BC, Canada

Ryan S Nicoll
Dynamic Systems Analysis Ltd.
Victoria, BC, Canada

¹Corresponding author: hlbailey@uvic.ca

ABSTRACT

This paper looks at the methodology of building a full wave-to-wire WEC (Wave Energy Converter) simulation and presents examples of its use for a variety of different types of WEC.

Wave resource information from the West Coast of Vancouver Island is considered. A detailed wave-body interaction model is generated using ProteusDS software. This model is linked to Simulink which allows a detailed PTO (Power Take Off) model to be simulated which will feedback into the motions of the WEC.

Three different examples are presented for different WECs. These WECs are Resolute Marine Energy's Surging flap, Seawood Designs' SurfPower and an internal University of Victoria two body concept.

NOMENCLATURE

A_n, A_{nCF} Nozzle area and the ideal nozzle area of a Pelton turbine for constant PTO force.
 A_{proj} Projected frontal area in the direction of the relative fluid flow.
 A_η A constant related to the motor efficiency
 B Smoothing constant.
 β Pelton turbine bucket angle.
 C_C Cross sectional area of the hydraulic cylinder.
 C_d Drag coefficient.
 C_v Nozzle loss coefficient.
 c_{PTOLim} Spring constant for the PTO limit module.
 D_M, D_{MCF} The displacement of the motor, and the ideal displacement of the motor for a constant PTO force.
 D_{mMax} The maximum displacement
 ΔP_{nom} The nominal pressure across the motor.

η_G Generator efficiency.
 F_{PTO}, F_{drag} PTO and drag force, respectively.
 F_{PTOLim} Force due to the PTO limit module.
 γ Adiabatic index, typically 1.4.
 J Motor inertia.
 k_{PTOLim} Damping constant for the PTO limit module.
 k_{LL}, k_{LP}, k_{LD} The loss coefficients for the variable displacement motor.
 $k_{L\infty}, k_{F1}, k_{FP}$
 $k_{FD}, k_{F\infty}$ Pressures; initial, high and low pressure at the hydraulic cylinder and the motor, respectively.
 P_0, P_{HC}, P_{LC}
 P_{HM}, P_{LM} The motor and generator power, respectively.
 p_m, p_G Volumetric fluid flow rate for the hydraulic piston and motor, respectively.
 q_C, q_m Distance from the fluid jet centerline to the shaft centerline of a Pelton turbine.
 r Density of hydraulic fluid.
 ρ Time and the time step.
 $t, \Delta t$ Generator and motor torque.
 T_G, T_m Initial volume and volume of fluid in the high and low pressure accumulator, respectively.
 V_0, V_H, V_L Relative fluid velocity.
 v The angular velocity and acceleration of the shaft.
 $\omega_m, \dot{\omega}_m$ The limit of angular acceleration of the shaft
 $\dot{\omega}_{mLim}$ The nominal angular velocity of the shaft.
 ω_{mNom} The relative position, the position for the resistive load module limit, and relative velocity of the hydraulic piston.
 x, x_0, \dot{x}

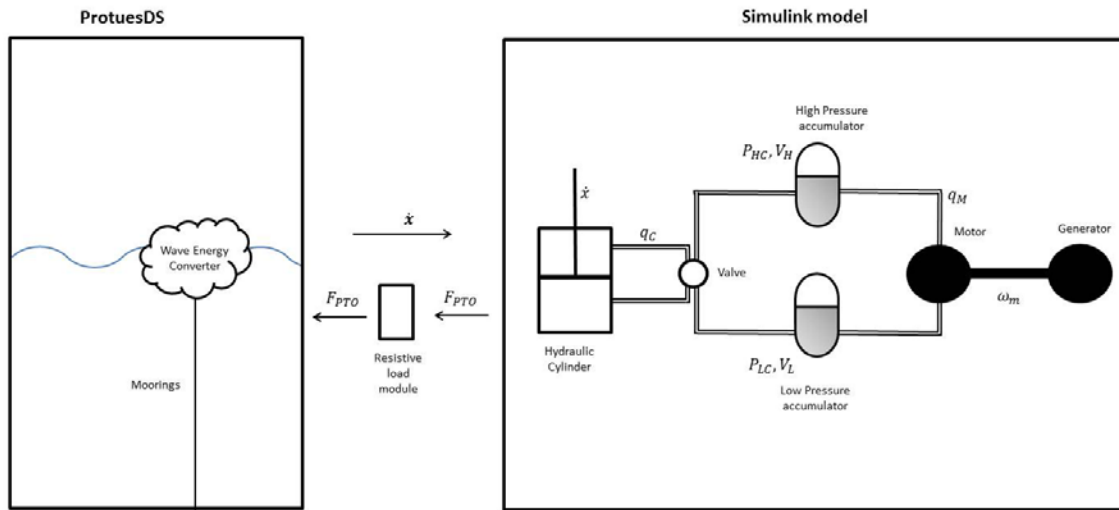


FIGURE 1. A SCHEMATIC OF THE SIMULATION

INTRODUCTION

This paper aims to present a methodology for developing a full wave to wire simulation for WECs. High fidelity simulations are needed to explore all the different dynamic effects that are occurring in these interrelated systems and to capture all the influences that have an effect on the resulting power extraction. This is shown schematically in Figure 1.

The methodology of this paper is being implemented for a number of different WECs. These developers are:

- Resolute Marine Energy, a surging flap WEC fixed to the seabed.
- Seawood Design Inc, a floating pontoon reacting against the seabed.
- UVic's internal WEC concept, a two body, float and spar WEC.

For a high fidelity wave-to-wire simulation, detailed wave conditions at the theoretical deployment site are required. This paper uses information from a Simulating Waves Near-shore (SWAN) [1] numerical model that utilizes hindcasted spectral wave conditions off the West Coast of Vancouver Island, BC, Canada from global wave and wind forecast models [2].

The incoming wave forces on the WEC need to be quantified as well as the forces resulting from the induced motion of the WEC, this includes the buoyancy forces, wave radiation forces, mooring forces and viscous drag forces. These forces, alongside the PTO force from an external model, are summated for each time step to determine future motions. This is implemented within the ProteusDS software package, with the option for some of the hydrodynamic parameters to be

obtained using WAMIT or SHIPM03D and imported into this software.

The PTO influences the WEC, its motions and the resulting power output [3] and must be modeled in the time domain due to the inherent nonlinearities in the system. The PTO characteristics will affect the WEC's power extraction capabilities, therefore to enable realistic values of power that can be transmitted to an electrical grid; high fidelity PTO simulations are required.

There are three typical PTO systems that can be used. Hydraulic, pneumatic or electrical [4] such as direct drive [5]. This paper only considers hydraulic PTO systems. Examples of considerations using a hydraulic PTO that have been published in scholarly works are by Pelamis [6], WaveStar [7], Oyster [8]. Generic research in using hydraulic PTO as part of WECs includes work by Ricci et al [9], Zhao et al [10], Cargo et al [11], among others.

Wave-to-wire simulations of different levels of complexity have been developed by a variety of authors such as Josset et al [12] and Garcia-Rosa et al [13].

This paper is separated into a number of sections. The different WEC's that are being used as examples will be presented, as well as the wave resource that is being considered. The details of the simulation of wave-body interactions and the PTO system are presented. Discussions on these simulations are provided along with sample simulation results and then conclusions are drawn.

WECS INVESTIGATED

This paper will demonstrate how the methodology has been applied to three different WECs. Exact details of the WECs will not be given, as they are just being used to show the broad applicability of this methodology, and the typical outputs.

Resolute Marine Energy

Resolute Marine Energy [14] is developing a surging flap type of WEC which operates in near shore locations (see Figure 2). The buoyant flap rotates about a fixed axis that is rigidly attached to the seabed. There is a hydraulic cylinder that operates between the flap and the fixed base. The motion of the flap compresses and expands this hydraulic cylinder. The pressurized fluid is then pumped to shore to operate, in this case, a variable displacement motor.



FIGURE 2: REPRESENTATION OF RESOLUTE MARINE ENERGY'S WEC

SurfPower

Seawood Designs Inc. [15] is developing a buoyant rectangular pontoon that floats on the water surface and is free to move in 5 degrees of freedom (see Figure 3). In these simulations it is locked in yaw and a yaw control mechanism is planned for real-world deployments. The buoyant float has dimensions of 24 m long, 7 m wide and a width of 1 m. The pontoon is attached to a hydraulic cylinder via a bridle. The hydraulic cylinder is fixed at its base to the ocean floor and it is able to rotate around this fixed point. In these simulations a water depth of 40 m is assumed. As the pontoon moves in the waves it expands and contracts the hydraulic cylinder that is located on the seabed; power is extracted only on the upstroke of the hydraulic piston.

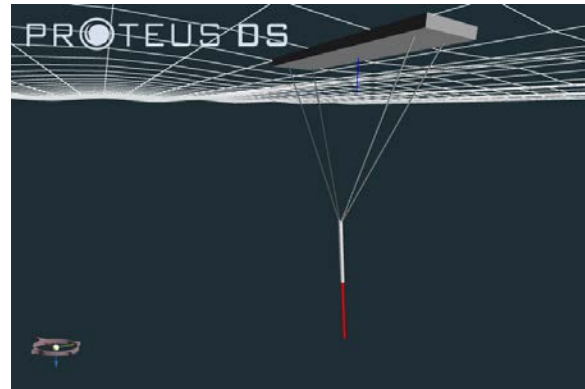


FIGURE 3: SURFPOWER

Two-body concept

UVic's internal concept [16] is a symmetric two body configuration, with a buoyant float co-axially aligned with a spar (see Figure 4). The spar is free to move in 6 degrees of freedom and the float can only move in one direction relative to the spar, along the co-axial axis. The PTO operates between these two bodies and the power is extracted for both directions of movement. The system is slack moored to the seabed. This concept is being used as a research platform for the University of Victoria.

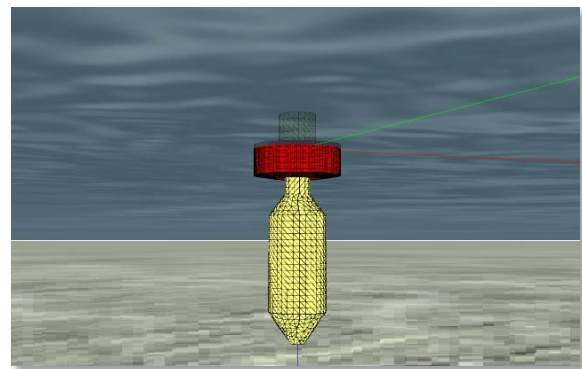


FIGURE 4: UVIC INTERNAL CONCEPT

WAVE RESOURCE INPUTS

The first step in the creation of a wave-to-wire model is to precisely determine the wave climate and characteristics in which the WEC's will be operating and from which power will be extracted. The spatial and temporal variation of the wave climate off Vancouver Island is dramatic and this variation must be quantified to ensure subsequent device design and tuning is done with the environmental conditions in mind.

Using a combination of deployed wave measurement buoys and numerical results from a SWAN model, the wave conditions off Vancouver Island have been hindcast for the last 10 years [2]. The model covers approximately 200 000 km² and features 280 000 computational nodes. This results in the spatial resolution of wave

characteristics in the nearshore, and general WEC operating ranges, to be approximately 200 m.

Amphitrite Bank, just 7 km offshore from the community of Ucluelet, has been the site of numerous initial investigations by WEC developers due to the localized increase in wave energy transport due to bathymetric energy convergence, see Figure 5.

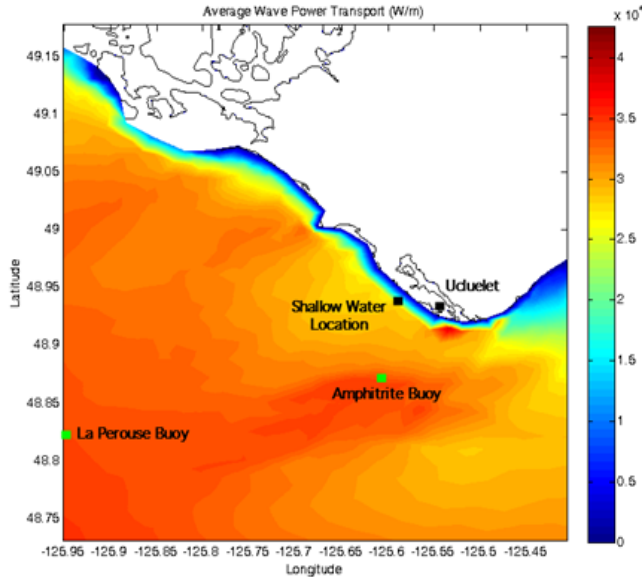


FIGURE 5: MEAN MODELED WAVE ENERGY TRANSPORT FOR THE YEAR 2010 AROUND AMPHITRITE BANK

The West Coast Wave Initiative (WCWI) has deployed a wave measurement buoy on Amphitrite Bank at 48.89° N 125.61° W in approximately 40 m of water depth. This location and the associated wave conditions will be used as a baseline location for all subsequent calculations since it is industrially relevant, close to shore and electrical transmission lines, and features significant annual wave energy transport (~ 40 kW/m).

For the purposes of demonstrating the performance of the wave-to-wire model, the sea state which contributes the highest percentage of wave energy transport to the annual total will be used as inputs: 2.75 m at 9.5 seconds. The bivariate distribution shown in Figure 6 details the occurrence frequency and energy distribution at the Amphitrite buoy location.

In order to determine the total annual potential power extraction by a WEC, the histogram of wave heights and periods above will be overlaid with a representative power matrix for each modelled device and the total power output calculated.

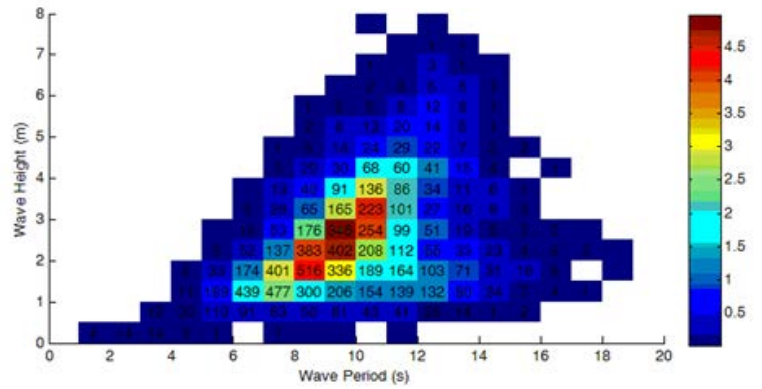


FIGURE 2: HISTOGRAM SHOWING THE OCCURRENCE FREQUENCY AND ENERGY DISTRIBUTION AT THE AMPHITRITE BUOY LOCATION. NUMBERS INDICATE THE NUMBER OF HOURS EACH YEAR, WHILE THE CONTOUR COLOURS INDICATE THE PERCENTAGE OF TOTAL ENERGY WITHIN THAT SEA STATE. COLOUR BAR IS IN PERCENTAGE (%)

WAVE FORCES, MOORINGS AND DRAG

The wave, mooring and drag forces are obtained from the time domain simulation software, ProteusDS.

The hulls of the bodies as defined in ProteusDS are subdivided into discrete surfaces represented by mesh panels. The Froude-Krylov force from the incoming waves is calculated on each panel with a wetted centroid and the pressure field used for this calculated is from equations provided by DNV documentation [17], this pressure field accounts for both buoyancy and the pressure field disturbance due to incoming wave forces. The incoming wave force (including the force from wave scattering) can also be calculated from hydrodynamic information provided by WAMIT or ShipMo3D.

The drag force is calculated for each panel based on a drag coefficient obtained from either experimental data or from empirical data of standard shapes. This is calculated as proportional to the square of the velocity difference between the fluid velocity and the panel's centroid's velocity in each orthogonal direction, for each panel area,[18] [19]. It is based on the standard equation of fluid drag

$$F_{drag} = \frac{1}{2} \rho C_d A_{proj} v^2 \quad (1)$$

where C_d is the drag coefficients, A_{proj} is the projected frontal area in the direction of the relative fluid flow and v is the relative fluid velocity.

The added mass can either be calculated using a similar method to the drag force, where an added mass coefficient is used from either

experimental data or from empirical data for standard shapes [17] or the added mass can be included in the radiation force calculation from WAMIT or ShopMo3D hydrodynamic parameters.

Moorings forces are calculated using a finite-element cable model, specifically it uses a cubic-spline lumped mass cable model [20]. The cable's material properties: the bending or flexural rigidity, the torsional rigidity and the axial rigidity are specified along the cable length.

Incoming waves can be modeled as either regular, also called Airy waves, or irregular waves from one direction or if irregular waves, using a directional spreading function. For irregular waves a seed value is used to ensure repeatable runs.

The forces are summated on the rigid bodies and the motions of the bodies are calculated for up to six degrees of freedom. The time-domain solver either uses an adaptive variable step size 4th/5th order Runge-Kutta method or a fixed step size 4th order Runge-Kutta method. In this paper, a variable step size was used as this provided the fastest possible solution without any problems associated with system stability.

PTO MODEL

The PTO simulation is modeled in the software package Simulink and it comprises a hydraulic piston, high and low pressure accumulators, a motor and a generator. A typical setup is schematically presented in Figure 1. This model is connected to ProteusDS using a *Simulink s-function* that linked to the force control module, which is written in C++, that then calls a DLL (Direct Library Link) provided by Dynamic Systems Analysis Ltd.

Hydraulic cylinder and accumulators

The PTO force is calculated from the product of the relative pressures, $(P_{HC} - P_{LC})$, across the hydraulic cylinder and its cross-sectional area, C_c , taking into account the sign of the hydraulic cylinder's velocity, \dot{x} , [21]

$$F_{PTO} = -(P_{HC} - P_{LC})C_c \text{sign}(\dot{x}) \quad (2)$$

The volumetric flow rate from the hydraulic piston to the high pressure accumulator and also from the low pressure cylinder back into the low pressure side of the hydraulic cylinder is [21],

$$q_c = \dot{x} C_c \quad (3)$$

The volume of fluid in the high and low pressure accumulators is then calculated from [11],

$$V_H = \int_0^t (q_c - q_m) dt \quad (4)$$

$$\& \\ V_L = \int_0^t (q_m - q_c) dt \quad (5)$$

where q_m is the volumetric flow rate through the motor.

The pressures in the gas accumulators can then be calculated from,

$$P = \frac{P_0 V_0^\gamma}{(V_0 - V_H)^\gamma} \quad (6)$$

where γ is the adiabatic index, P_0 is the initial pre-charge pressure, and V_0 is the volume of the accumulator which is also equal to the initial volume of gas in the accumulator.

The pressure loss due to the inertia and viscosity of the fluid, either between the hydraulic cylinder and accumulators and / or the accumulators and the motor, and the effect of valves has not been included in this model.

Motor

Two different types of motor can be considered to transform the hydraulic pressure into rotational motion. These motors are the variable displacement motor and the Pelton turbine.

The variable displacement motor

The flow through the motor is calculated from Equation 7 which also includes the volumetric losses due to some of the fluid not doing work on the motor [22],

$$q_m = D_m \omega_m - q_{losses} \quad (7)$$

where the angular velocity of the motor shaft is ω_m , and the variable displacement of the motor is D_m . The losses, q_{losses} are calculated from

$$q_{losses} = D_m \omega_m k_{L1} \left(\frac{P_{HM} - P_{LM}}{\Delta P_{nom}} \right)^{k_{LP}} \times \left(\frac{D_m}{D_{mMax}} \right)^{k_{LD}} \left(\frac{\omega_m}{\omega_{mNom}} \right)^{k_{L\infty}} \quad (8)$$

where k_{L1} , k_{LP} , k_{LD} & $k_{L\infty}$ are coefficients associated with a particular motor's efficiencies. ΔP_{nom} and ω_{mNom} are the nominal values for the pressure difference across the motor and the motor rotational speed, and D_{mMax} is the maximum displacement of the motor.

The torque produced by this variable displacement motor can then be calculated from:

$$T_m = (P_{HM} - P_{LM})D_m - T_{losses} \quad (9)$$

T_{losses} are the mechanical losses which are calculated from,

$$T_{losses} = D_m \Delta P k_{F1} \left(\frac{P_{HM} - P_{LM}}{\Delta P_{nom}} \right)^{k_{FP}} \times \left(\frac{D_m}{D_{mMax}} \right)^{k_{FD}} \left(\frac{\omega_m}{\omega_{mNom}} \right)^{k_{F\infty}} \quad (10)$$

where k_{F1} , k_{FP} , k_{FD} & $k_{F\infty}$ are the motor specific coefficients of the mechanical losses.

The power from the variable displacement motor is then calculated from,

$$P_m = D_m \Delta P \omega_m \quad (11)$$

The variation in the variable displacement, D_m , of the motor affects both the output power and the pressure across it. For constant output power, the product of both D_m and the relative pressure across the hydraulic cylinder need to be a constant (assuming that there is enough flow rate though the motor and that a fixed speed generator is present), as presented in Equation 11. This is desirable as it produces a smooth flow of electricity into the electrical grid.

A constant PTO force allows the WEC to have a predetermined resistance which can be tuned to optimize the power extraction for certain sea states. However, this will result in a highly variable power output. To keep a constant PTO force, D_m would be calculated from,

$$D_m = D_{mCF} = \frac{q_c}{\omega_m} \quad (12)$$

where D_{mCF} is the displacement that resulted in a constant force.

Variations in D_m could be focused upon either smoothing the power output or providing the ideal PTO force. The method used in this work is to introduce a smoothing constant, B , such that D_m varies over time, as such,

$$D_m(t + \Delta t) = B D_m(t) + (1 - B) D_{mCF}(t) \quad (13)$$

where B is set between 0 and 1, and Δt is the simulation time step.

The angular acceleration of the shaft can then be calculated by the difference of the motor and generator torque divided by the combined rotational inertia, J , of the motor, generator and shaft,

$$\dot{\omega}_m = \frac{T_m - T_G}{J} \quad (14)$$

The Pelton Turbine

The velocity of the jet that hits the Pelton turbine V_j is calculated from [23],

$$V_j = C_v \left(\frac{2P_{HM}}{\rho} \right)^{1/2} \quad (15)$$

where C_v is the velocity coefficient that considers the losses associated with an imperfect nozzle, and is typically in the region of 0.92 to 0.98. ρ is the density of the hydraulic fluid, which could be water. This leads to the volumetric flow rate of the hydraulic fluid that flows through the motor being obtained from Equation 16.

$$q_m = A_n V_j \quad (16)$$

where A_n is the cross sectional area of the nozzle.

The power of a Pelton turbine is calculated from,

$$p_m = 2\pi r \omega_m \rho q_m (V_j - 2\pi r \omega_m) (1 - \cos \beta) \quad (17)$$

where β is the bucket angle of the turbine, typically c. 165 degrees and r is the distance to the jet centerline from the shaft centerline.

As with the variable displacement motor, one method of varying A_n would try to produce a constant power flow while another would try to produce a constant PTO force. For a constant PTO force, the value of A_n would be,

$$A_{nCF} = \frac{q_c}{V_j} \quad (18)$$

Similarly to the treatment of the variable displacement motor, we introduce the smoothing constant B , that is valued at between zero and one, into the simulation.

$$A_n(t + \Delta t) = B A_n(t) + (1 - B) A_{nCF}(t) \quad (19)$$

The torque generated on the shaft from the Pelton turbine is calculated from

$$T_m = 2\pi r q_m \rho (1 - \cos \beta) (V_j - 2\pi r \omega_m) \quad (20)$$

The angular acceleration of the shaft can then be generated in the same manner as in Equation 14.

Generator

The generator can have a variable speed or a fixed speed. Examples of a variable speed generator are a DFIG or a variable speed asynchronous generator. Fixed speed generators could be a synchronous generator or an asynchronous generator which operates very

close to a fixed speed and for this work, we would consider as a fixed speed generator.

Fixed speed generator

The torque of a fixed speed generator perfectly matches the motor torque, this results in the power output to the electricity grid to be equal to

$$P_G = \eta_G T_G \omega_m \quad (21)$$

where η_G is the efficiency of the generator.

Variable speed generator

The torque of the variable speed generator is allowed to vary relative to the torque of the motor. This is to allow a limited a rate of change of the shaft's angular velocity, $\dot{\omega}_{mLim}$, within the range of a minimum and maximum value. The change is done in the direction that increases the efficiencies of the variable displacement motor or the impulse turbine. This value is chosen to allow a slow change in the shaft speed, on the order of minutes, so as to not affect the power smoothness too significantly. This also slowly increases the WEC's efficiency. The generator torque that is required to achieve this is

$$T_G = T_m + A_\eta J \dot{\omega}_{mLim} \quad (22)$$

where A_η is 1 for when the efficiency of the motor would increase with a decreased shaft speed, and minus 1, for when the efficiency of the motor would increase with an increased shaft speed.

The power output for a variable speed generator is calculated as a 30 second running average of the output of Equation 19 [24].

Resistive Force module

The ProteusDS simulation runs at smaller time steps than the Simulink simulation and to reduce simulation time we typically run it with a variable step size Runge-Kutta solver. The computational time cost of having the Simulink simulation run at the same speed is too high. Therefore in the link between them, the effective coulomb damping of the PTO needs to be modeled to ensure that it is a purely resistive load and does not impart motion to the WEC. So if the resistive force module was not used, the PTO force would potentially accelerate the body in the opposite direction to its current velocity, potentially resulting in an unstable system.

To attempt to achieve this, the PTO force is modeled as a linear spring and damper when its magnitude should be less than the total resistive force,

$$F_{PTOLim} = -(k_{PTOLim}(x - x_0) + c_{PTOLim}\dot{x}) \quad (23)$$

where k_{PTOLim} is the linear spring constant and c_{PTOLim} is the linear damping constant. The value of x_0 is originally the initial position of the cylinder, which gets updated as described below.

When the motion of the WEC is such that the PTO force is fully resistive to motion, then the PTO force remains un-altered.

If the value of F_{PTO} is smaller than the value of F_{PTOLim} then the PTO force fed into the ProteusDS simulation is F_{PTO} of Equation (2). In turn, the value of x_0 is then updated as the new position of the hydraulic cylinder as long as this new value isn't greater in magnitude than the sum of the old x_0 and F_{PTO}/k_{PTOLim} . If this is the case, then the previous value of x_0 is kept.

Care needs to be taken in the choice of c_{PTOLim} and k_{PTOLim} as they need to allow the PTO force to be fully developed when the WEC is in motion but not to impart motion to the WEC.

DISCUSSIONS

Varying D_m and the effect on power and ΔP

Simulation runs were conducted with varying values of smoothing constant, B . In these simulations, in order to focus the results on the variation of B , the mechanical and volumetric losses in the motor were eliminated, i.e. k_{F1} and k_{L1} were set to 0. The size of the accumulators' affects the results, so the accumulators were kept consistent across the different runs tested to allow focus on the variation of B . The volume of the accumulators was chosen so that they always had less than 10% of their total volume was occupied by the hydraulic fluid. When B was set to 1 they tended to approach this 10% limit.

B	Standard Deviation / mean(abs)			Standard Deviation
	D_m	F_{PTO}	p_m	\dot{p}_m
0	0.00	1.27	0.78	0.109
$1 \times 10^{-4} \Delta t$	0.03	1.28	0.80	0.111
$1 \times 10^{-3} \Delta t$	0.24	1.29	0.88	0.128
$1 \times 10^{-2} \Delta t$	0.87	1.21	1.29	0.384
1	1.34	0.99	1.34	0.152

TABLE 1: THE VARIATIONS OF $D_m, F_{PTO}, \& P_m$ WITH RESPECT TO B .

B was set at 0, $1 \times 10^{-4} \Delta t$, $1 \times 10^{-3} \Delta t$, $1 \times 10^{-2} \Delta t$ and 1, where the time step, Δt , was $1/300$ s. These simulations were run for 200 s in the same JONSWAP sea state. The resulting D_m , the pressure across the cylinder and the motor power are presented in Figure 8, for the first 50 s. A

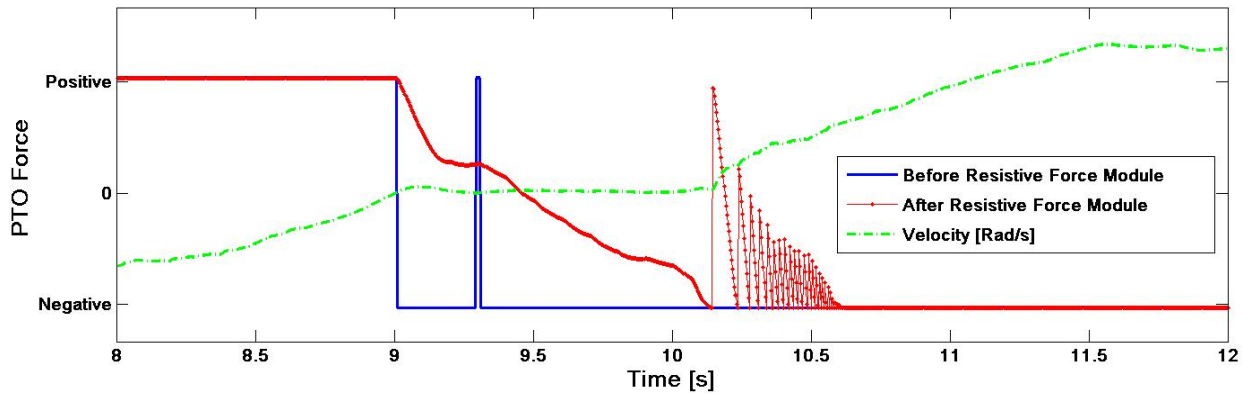


FIGURE 3: THE AFFECT OF THE RESISTIVE FORCE MODULE

statistical analysis of the motions for the 200 s runs are presented in Table 1. This table presents the standard deviation, for each of the parameters of interest, divided by the mean of the absolute values, and the standard deviation of the derivative of the power. The table and figure together show that to achieve a smooth PTO force, B should be one, which results in a highly variable D_m . The smoothest power output occurs, in this case, when B is zero. It is noted that keeping a constant D_m does not directly result in a smooth power output due to the pressure variations. Setting D_m to a varying value based on the known accumulator pressures and volumetric fluid flow into the high pressure accumulator that would result in a constant power output would potentially be preferable and this is an area of future research.

Resistive Force module

This section looks at the effect of using the resistive force module to vary the PTO force that is fed into the ProteusDS simulation. The constants, c_{PTOLim} and k_{PTOLim} will have an effect on the simulation and need to be chosen so that they allow the full resistive force of the PTO while the body is in motion, but do not provide a force to the body while it should be stationary.

These values are obtained by a combination of trial and error, and consideration of the damping ratio. The simulation was run for one of the WECs studied and the PTO force entering and leaving the resistive force module is presented in Figure 7. The constants used were $k_{PTOLim} = \frac{F_{PTO}}{0.001}$ and $c_{PTOLim} = \frac{F_{PTO}}{0.03}$. It can be seen that for c. 8-9 seconds, when the body has a negative velocity the PTO force resists motion with a constant force. When the body has approximately zero velocity at c.9-10 seconds, the PTO force experienced is less than the force from the hydraulic cylinder due to the resistive force module. At c.10 - 10.5 seconds,

there are some high frequency oscillations due to the velocity becoming non-zero and the value of x_0 changing; this variation in the PTO force is a limitation of this technique, which rapidly decays. After 10.5 seconds the PTO force from the resistive force module is the same as is input to it.

EXAMPLE SIMULATIONS

All the different WECs considered in this paper are simulated in a 2.75 m significant wave height, 9.5 s period wave spectrum. This spectrum has been previously identified as the most energetic contributor to the gross annual wave energy for the West Coast of Vancouver Island [2], with the identical wave time series used for all runs. For consistency this was used for all the devices even though Resolute Marine Energy's WEC is to be located in shallow water and this would affect the wave climate that it experiences. These simulations were run for 200 s.

The majority of the simulation results have had their output normalized in order to concentrate on the methodology and the different configurations that are possible as opposed to directly comparing different WECs.

Resolute Marine Energy's Surging Flap

For these simulations, we are using, high and low pressure accumulators, and a variable displacement motor connected to a fixed speed generator.

The simulation constants used are in Table 2, and the total volume of the accumulators used was such that they approached but were not greater than half full of fluid.

The simulation results are presented in Figure 9. The subfigures are clearly marked on the y-axis and they are, (in anti-clockwise order),

- the normalized velocity of the hydraulic piston.
- The normalized PTO force.

- The normalized volumetric flow rate that occurs from the hydraulic cylinder into and away from the high and low pressure accumulator, respectively; the volumetric flow through the variable displacement motor and the volumetric flow lost in the motor.
- The normalized power extracted, with the mechanical power being the total power extracted from the waves; the motor power refers to the useful power produced by the motor and the generator power is the power that is fed into an electrical grid.
- The pressure in the high and low pressure accumulators
- The efficiency of the variable displacement motor
- The value of D_m .

These simulation results show the variation in the PTO force resulting from the accumulator sizing, the choice of B and the variation in D_m . The visual correlation between D_m and the motor efficiency emphasizes how the value of D_m can influence the motor efficiency.

SeaWood Designs' SurfPower

The example case for SeaWood Designs' SurfPower WEC presented in this paper consists of a single SurfPower unit connected to a Pelton turbine and a fixed speed generator (although SurfPower units would typically be deployed in farms, which would smooth the fluid pressure and therefore increase the Pelton turbine's efficiency). A high pressure accumulator was incorporated into the system between the hydraulic cylinder and the motor to provide pressure smoothing. Seawater would be used for the hydraulic cylinder intake, so effectively an infinitely large low pressure accumulator is used.

The PTO values are as in Table 2, and the total volume of the high pressure accumulator is such that the accumulator is not more than one third full.

These results of these simulations are presented in Figure 10 where the subfigures are similar to those presented in Figure 9, and discussed above.

For this exact simulation, the variation of the turbine efficiency is lower than the efficiency variation of the other two cases with a variable displacement motor.

UVic's internal WEC concept

The example case for the UVic device uses a high and low pressure accumulator, a variable displacement motor and a variable speed generator. The excitation and radiation forces, for this example, are obtained from WAMIT.

The simulation is run with the variables in Table 2 and the maximum hydraulic fluid in the accumulators is less than 40% of their maximum capacity.

These results are presented in Figure 11, with the subfigures showing named quantities of interest. The subfigures are as described above except there is an additional subfigure showing the variable shaft speed.

In these simulations, the shaft speed of the generator varies in an attempt to increase the efficiency of the variable displacement motor and reaches its minimum shaft speed.

		Constant	Value used in these simulations
	Generator & motor inertia	J [kg/m ²]	20
Pelton Turbine	Nozzle efficiency	C_v []	0.95
	Bucket angle	β [deg]	165
Variable displacement motor	Coefficients	K_{LP} []	0.65
		k_{LD} []	-0.8
		$k_{L\omega}$ []	-0.2
		k_{FP} []	-0.65
		k_{FD} []	-0.75
		$k_{F\omega}$ []	0.2
		k_{L1} []	0.05
		k_{F1} []	0.06
	Generator efficiency	η_G []	0.98
	Smoothing constant	B []	$1 \times 10^{-5} \Delta t$

TABLE 2: PTO SIMULATION VALUES

CONCLUSIONS

A method of producing a wave-to-wire simulation of different WECs has been presented. The wave resource, the hydrodynamic wave interaction model and the PTO model has been discussed. Typical results have been presented for a number of different WECs with different PTO configurations.

ACKNOWLEDGEMENTS

The authors would like to acknowledge Resolute Marine Energy and Seawood Designs Inc. for their participation in the West Coast Wave

Initiative and allowing this information to be published.

Additionally the authors would like to acknowledge Natural Resources Canada, the Pacific Institute of Climate Solutions and the Natural Sciences and Research Council of Canada.

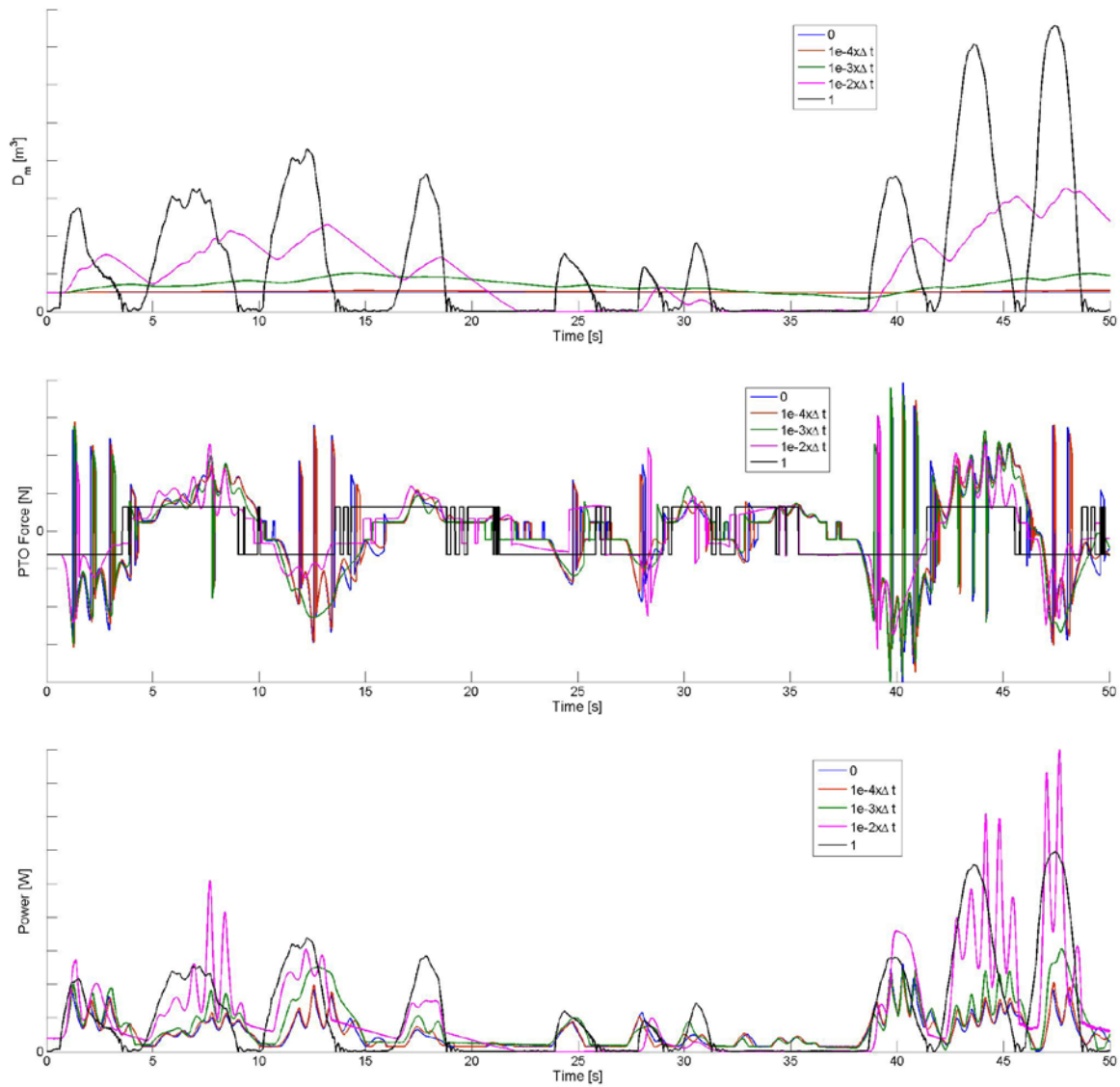


FIGURE 4: THE INFLUENCE OF B ON D_M , PTO FORCE AND MOTOR POWER

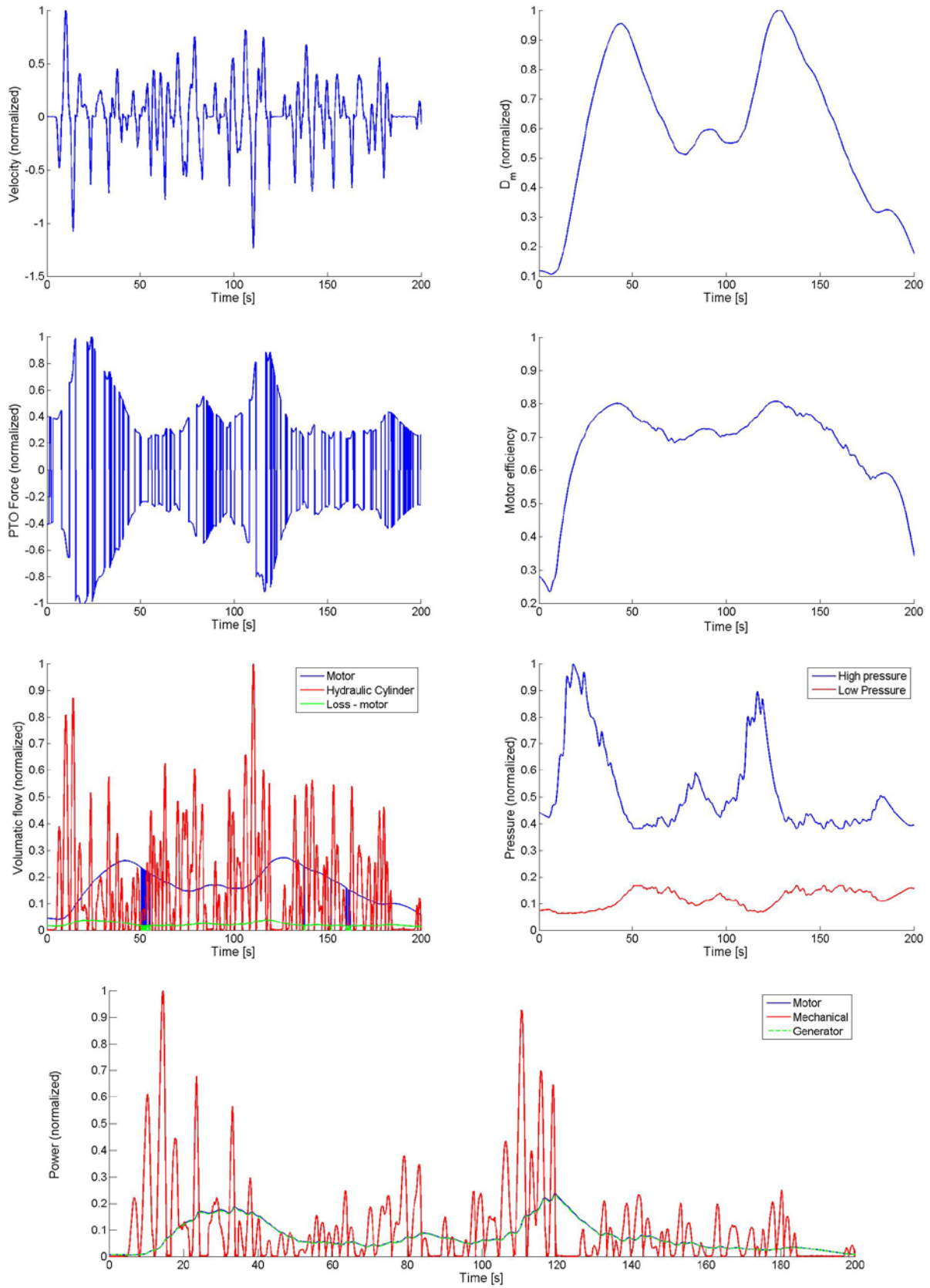


FIGURE 5: RESOLUTE MARINE ENERGY SIMULATION RESULTS

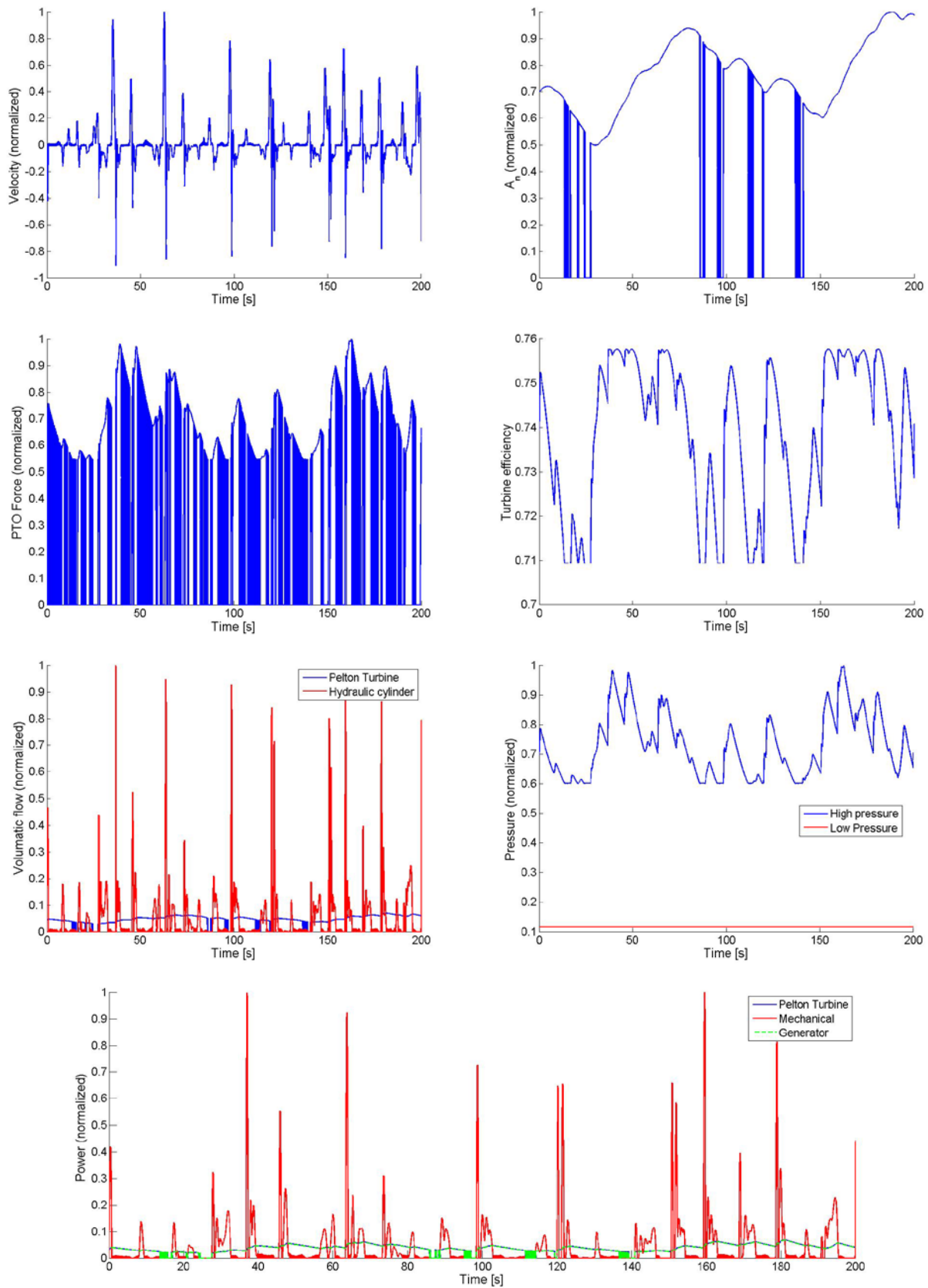


FIGURE 6: SURFPOWER SIMULATION RESULTS

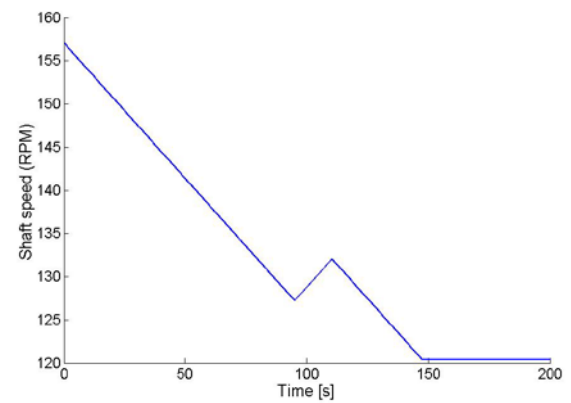
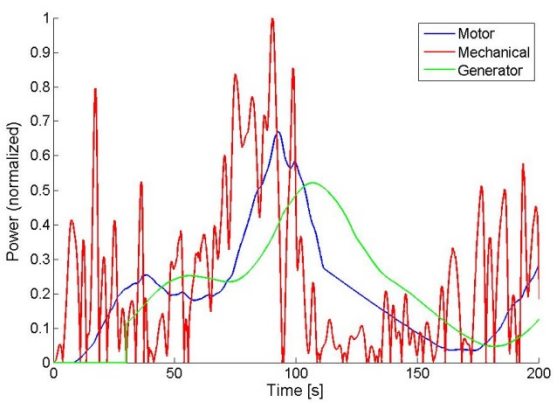
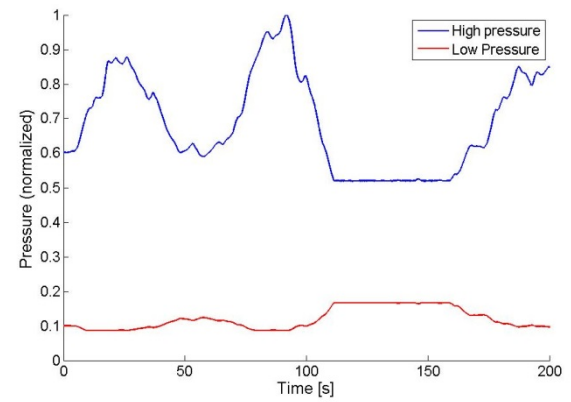
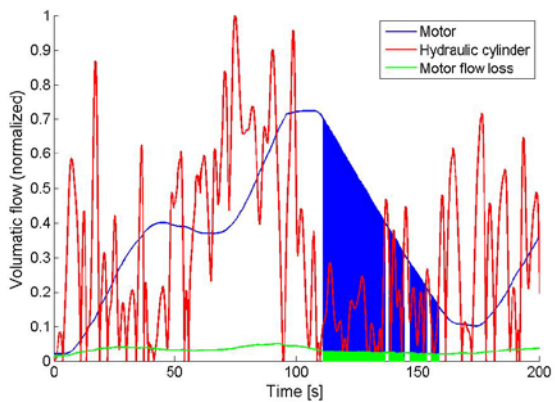
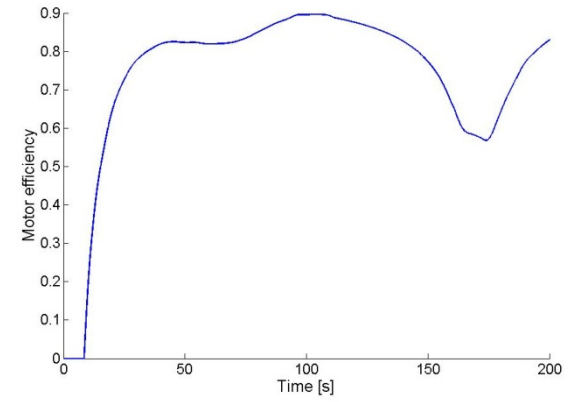
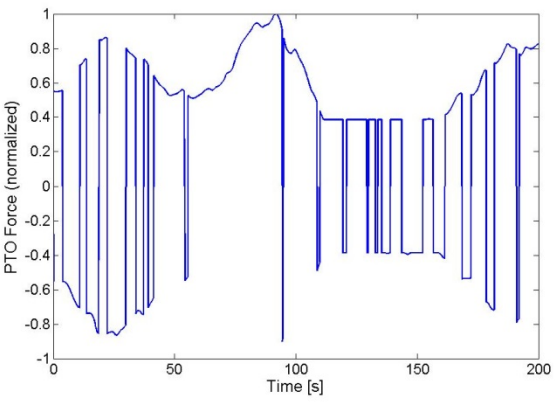
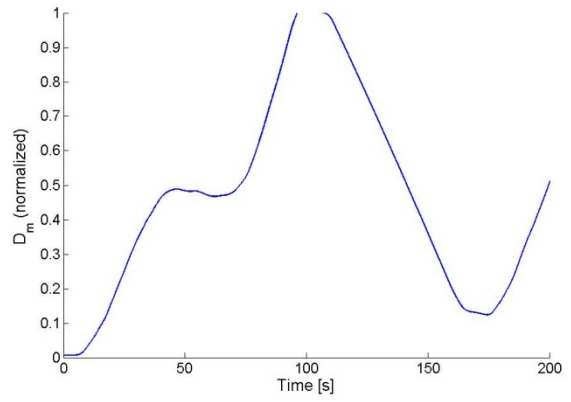
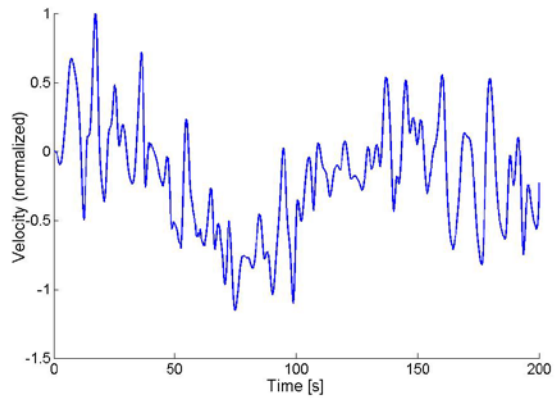


FIGURE 7: UVICS WEC CONCEPT

REFERENCES

- [1] N. Booij, L. H. Holthuijsen, and R. C. Ris, "The 'SWAN' wave model for shallow water.," in *Coastal Engineering Proceedings* 1.25, 1996.
- [2] B. Robertson, C. Hiles, and B. Buckham, "Characterizing the Nearshore Wave Energy Resource on the West Coast of Vancouver Island.," *Renew. Energy*, vol. In submiss, 2013.
- [3] H. Bailey and I. G. Bryden, "Influence of a quadratic power take-off on the behaviour of a self-contained inertial referenced wave energy converter," *Proc. Inst. Mech. Eng. Part M J. Eng. Marit. Environ.*, vol. 226, no. 1, pp. 15–22, Nov. 2011.
- [4] A. A. E. Price, "Classification of Wave Energy Converters by Power Flow," in *EWTEC*, 2013.
- [5] E. Spooner and M. A. Mueller, *Comparative study of linear generators and hydraulic systems for wave energy conversion*. Harwell Laboratory, Energy Technology Support Unit, 2001.
- [6] R. Henderson, "Design, simulation, and testing of a novel hydraulic power take-off system for the Pelamis wave energy converter," *Renew. Energy*, vol. 31, pp. 271–283, 2006.
- [7] R. Hansen, M. Kramer, and E. Vidal, "Discrete Displacement Hydraulic Power Take-Off System for the Wavestar Wave Energy Converter," *Energies*, vol. 6, no. 8, pp. 4001–4044, Aug. 2013.
- [8] T. Whittaker and M. Folley, "Nearshore oscillating wave surge converters and the development of Oyster.," *Philos. Trans. A. Math. Phys. Eng. Sci.*, vol. 370, no. 1959, pp. 345–64, Jan. 2012.
- [9] P. Ricci, J. Lopez, M. Santos, J. L. Villate, F. Salcedo, and A. Falcao, "Control Strategies for a simple Point-Absorber Connected to a Hydraulic Power Take-off," in *EWTEC*, 2009, pp. 746–755.
- [10] Q. Zhao and F. Gao, "Bond graph modelling of hydraulic six-degree-of-freedom motion simulator," *Proc. Inst. Mech. Eng. Part C J. Mech. Eng. Sci.*, vol. 226, no. 12, pp. 2887–2901, Feb. 2012.
- [11] C. J. Cargo, a. R. Plummer, a. J. Hillis, and M. Schlotter, "Determination of optimal parameters for a hydraulic power take-off unit of a wave energy converter in regular waves," *Proc. Inst. Mech. Eng. Part A J. Power Energy*, vol. 226, no. 1, pp. 98–111, Oct. 2011.
- [12] C. Josset, A. Babarit, and A. H. Clément, "A wave-to-wire model of the SEAREV wave energy converter," *Proc. Inst. Mech. Eng. Part M J. Eng. Marit. Environ.*, vol. 221, no. 2, pp. 81–93, Jan. 2007.
- [13] P. B. Garcia-Rosa, J. P. Soares Vilela, F. Lizarralde, S. F. Estefen, I. R. Machado, and E. H. Watanabe, "Wave-to-Wire Model and Energy Storage Analysis of an Ocean Wave Energy Hyperbaric Converter," *IEEE J. Ocean. Eng.*, 2013.
- [14] "Resolute Marine Energy Website," *Accessed: Jan 2014*. [Online]. Available: <http://www.resolutemarine.com/>.
- [15] "SeaWood Design's website," *Accessed: Jan 2014*. [Online]. Available: <http://www.surfpower.ca/>.
- [16] S. J. Beatty, B. J. Buckham, and P. Wild, "Frequency Response Tuning for a Two-Body Heaving Wave Energy Converter," in *ISOPE*, 2008, vol. i, pp. 342–349.
- [17] DNV, *Recommended practice DNV-RP-C205 environmental conditions and environmental loads*. 2010, p. Table 3–1.
- [18] R. S. Nicoll, C. F. Wood, and A. R. Roy, "Comparison of Physical Model Tests With a Time Domain Simulation Model of a Wave Energy Converter," in *ASME 2012 31st International Conference on Ocean, Offshore and Arctic Engineering. American Society of Mechanical Engineers*, 2012.
- [19] D. Bull and P. Jacob, "Methodology for creating nonaxisymmetric WECs to screen mooring designs using a Morison Equation approach," *Ocean. 2012*, pp. 1–9.

- [20] B. J. Buckham, "Dynamics modelling of low-tension tethers for submerged remotely operated vehicles," University of Victoria, 2003.
- [21] A. F. de O. Falcão, "Modelling and control of oscillating-body wave energy converters with hydraulic power take-off and gas accumulator," *Ocean Eng.*, vol. 34, no. 14–15, pp. 2021–2032, Oct. 2007.
- [22] "MATLAB and SimHydraulics Toolbox Release 2013a, The MathWorks, Inc., Natick, Massachusetts, United States."
- [23] F. M. White, *Fluid Mechanics*, 4th ed. McGraw-Hill, 1999.
- [24] J. Duquette, D. O. Sullivan, S. Ceballos, and R. Alcorn, "Design and Construction of an Experimental Wave Energy Device Emulator Test Rig," 2009.